International Symposium
On Turbulence and Shear Flow
Phenomena (TSFP-8)
August 28 - 30, 2013 Poitiers, France

VORTEX SHEDDING IN A VARICOSE MODE BEHIND A RISING BUBBLE

Márcio-Ricardo Pivello
FEMEC - UFU
Av. João Naves de Ávila, 2121,
Campus Santa Mônica Bloco 5P
Uberlândia, MG, Brazil
pivello@mecanica.ufu.br

Millena Martins Villar Valle
FEMEC - UFU
Av. João Naves de Ávila, 2121,
Campus Santa Mônica Bloco 5P
Uberlândia, MG, Brazil
mmvillar@mecanica.ufu.br

Alexandre M. Roma
IME - USP
Rua do Matão, 1010,
Cidade Universitária,
São Paulo, SP, Brazil
roma@ime.usp.br

Aristeu da Silveira-Neto
FEMEC - UFU
Av. João Naves de Ávila, 2121,
Campus Santa Mônica Bloco 5P
Uberlândia, MG, Brazil
aristeus@mecanica.ufu.br

ABSTRACT

This work presents a computational methodology for the simulation of three-dimensional, two-phase flows, based on adaptive strategies for space discretization, as well as a varying time-step approach. The method is based on the Front-Tracking Method and the discretization of the *Eulerian* domain employs a Structured Adaptive Mesh Refinement strategy along with an implicit-explicit pressure correction scheme. Modelling of the *Lagrangian* interface was carried out with the GNU Triangulated Surface (GTS) library, which greatly reduced the difficulties of interface handling in 3D. The methodology was applied to a series of rising bubble simulations and validated employing experimental results and compared to literature. Finally, the algorithm was applied to the simulation of two cases of bubbles rising in the wobbling regime. The use of adaptive mesh refinement strategies led to physically insightful results, which otherwise would not be possible in a serial code with a uniform mesh.

INTRODUCTION

A bubble rising in a quiescent liquid reaches its terminal velocity when the forces acting on it (drag, buoyancy and weight) are in equilibrium. However, unlike rigid bodies, deformation can take place as a result of the surrounding flow and, also, the transfer of momentum across the interface may induce vortices inside the bubble. Therefore, the bubble shape will depend on the viscous forces, interface forces, and also on the forces from the surrounding flow (de Vries, 2001).

Rising bubble flows can be described in terms of three non-dimensional numbers: the Eötvos number, $Eo = g\Delta\rho\phi^2/\sigma$, the Morton number, $M = g\Delta\rho\mu_c^4/\rho_c^2\sigma^3$ and the Reynolds number, $Re = \rho_c U\phi/\mu_c$, where g is the gravity acceleration, ρ_c is the density of the continuous phase, $\Delta\rho$ is the difference between densities of the continuous and disperse phases, ϕ is the equivalent diameter of the bubble, μ_c is the dynamic viscosity of the continuous phase, U is the characteristic bubble velocity and σ is the interface tension related to the fluid-fluid interface.

Bubbles tend to deform when subjected to external flow fields until normal and shear stresses balance at the fluid-fluid interface. Their shape under the action of gravity in an initially quiescent liquid can be grouped into three large categories: spherical, ellipsoidal and spherical- or ellipsoidal-cap. If the interfacial tension and/or viscous forces are much more significant than inertial forces, bubbles are termed *spherical*. Clift *et al.* (1978) classify a rising bubble as spherical if its height to width ratio lies within 10% of unity. *Ellipsoidal* bubbles are oblate with a convex shape when viewed from inside and may present axisymmetry. As inertia forces become more important, ellipsoidal bubbles may undergo periodic dilatation or random wobbling motion, making shape characterization a difficult task (Bhaga & Weber, 1981). Large bubbles usually have flat or indented bases, without fore-and-aft symmetry. Their fore-shape may resemble segments oblate spheroids of low eccentricity, thence the names *spherical-cap* or *ellipsoidal-cap*. Bubbles in this regime may also develop thin envelopes of dispersed fluid at their bases, usually referred to as skirts (Brennen, 2005).

In the present work, the motion of a single bubble rising in an otherwise quiescent liquid was simulated under two different configurations, both leading to an unsteady path. The simulations were carried out using a Front-Tracking Method coupled with a Structured Adaptive Mesh Refinement for solving the Navier-Stokes equations.

The Front-Tracking (FT) Method of Tryggvason (Unverdi & Tryggvason, 1992; Tryggvason *et al.*, 2001) is based on the One-Fluid Formulation (OFF) and on the Immersed Boundary (IB) Method of Peskin (1977, 2002).

In the OFF approach, the Navier-Stokes equations are solved as if a single fluid, with space-dependent physical

properties, were used. The presence of the fluid-fluid interface is modelled using a source term for the interface tension force, as shown in Eqs. 1 and 2 below.

$$\rho[\frac{\partial \mathbf{u}}{\partial t} + (\mathbf{u}\cdot\nabla)\mathbf{u}] = \nabla\cdot[\mu(\nabla\mathbf{u} + \nabla\mathbf{u}^T)] + \\ -\nabla p + \rho\mathbf{g} + \mathbf{f}_\sigma, \quad (1)$$

$$\nabla\cdot\mathbf{u} = 0. \quad (2)$$

The interface is represented by an unstructured, triangulated *Lagrangian* surface mesh, on which the interface force is calculated by integrating the interface tension on a surface element ΔS, as $\delta\mathbf{F}_\sigma = \int_{\Delta S}\sigma\kappa\mathbf{n}ds$, where σ is the surface tension coefficient, κ is twice the mean curvature for three-dimensional domains and $\mathbf{n}$ is the local normal to the surface. By replacing the geometrical relation $\kappa\mathbf{n} = (\mathbf{n}\times\nabla)\times\mathbf{n}$ (Tryggvason *et al.*, 2011) on this equation and using the Stokes theorem, the force on a surface element can be computed without explicitly calculating the surface curvature, via

$$\delta\mathbf{F}_\sigma = \oint_{\delta\Gamma}\sigma\mathbf{t}\times\mathbf{n}d\Gamma, \quad (3)$$

where $\delta\Gamma$ is the boundary of the integration element, $\mathbf{t}$ is the unit tangent and $\mathbf{n}$ is the outward unit normal, both computed at the element boundary. Integration of Eq. 3 is performed using the mesh triangles as integration elements, following the approach of Shin & Juric (2002), which leads to the following expression (indices are not related to Einstein notation):

$$\mathbf{F} = \sum_j \sigma(\mathbf{t}_j\times\mathbf{n}_j), \quad (4)$$

where $\mathbf{F}$ is the vector force acting on a given element, $\mathbf{n}_j$ is the outer unit-normal associated to edge j and $\mathbf{t}_j$ is the non-normalized tangent vector at edge j.

After being computed on the interface mesh, the force is spread on the *Eulerian* referential, as in the IB Method (Peskin, 2002), in the vicinity of the interface position. The Navier-Stokes equations can then be solved, yielding the pressure and velocity fields. Interface advection is performed in a *Lagrangian* fashion, using the velocity field interpolated from the *Eulerian* domain onto the mesh surface vertices.

Interpolation and spreading processes are performed as described in (Tryggvason *et al.*, 2001), using the following equation as a Dirac kernel (Peskin, 1977):

$$W(r) = \begin{cases} \frac{1}{4}(1+cos(\frac{\pi}{2}r)), & r<2, \\ 0, & r\geq 2, \end{cases} \quad (5)$$

where $r = (x-X)/(h_x), (y-Y)/(h_y), (z-Z)/(h_z)$.

Physical properties such as viscosity and density are not literally advected. Instead, the position of the *Lagrangian* interface, explicitly tracked in time, is used to locate the constant, but different, material properties defined in the interior and exterior of the bubble. This is achieved by means of an indicator function, which yields a scalar field associated to each flow phase. In the present work, an approach based on the Closest Point Transform, or CPT, (Mauch, 2003) was used. Initially, CPT was developed as a means to create an implicit representation of a surface by computing its distance field. Ceniceros & Roma (2005) proposed an indicator function based on CPT, in which the distance computation is limited to an interval $[-\gamma,+\gamma]$, where γ is the absolute value of the largest distance from the interface to a given point in the Eulerian domain. The remaining of the domain is assigned with a constant value (e.g.: $+\gamma$ inside the dispersed phase and $-\gamma$ outside it). The distance field is not used directly. Instead, a smoothed Heaviside function is applied to it, so that the interval $[-\gamma,+\gamma]$ is mapped to [0, 1]. Then, any scalar field ψ can be computed as $\psi(\varphi) = H(\varphi)\psi_1 + (1-H(\varphi))\psi_2$, where the property ψ has value ψ_1 inside the bubble and ψ_2 elsewhere.

RESULTS

The numerical method was firstly verified using the *manufactured solutions* approach of Roache (1998), and then validation against experimental results was performed.

In all cases, velocity boundary conditions consisted of free-slip at the side boundaries, homogeneous Dirichlet at the bottom boundary, and homogeneous Neumann at the top boundary. Pressure boundary conditions consisted in homogeneous Neumann at the side and bottom boundaries, while homogeneous Dirichlet was used at the top boundary. *Eulerian* grid refinements were based on the position of the *Lagrangian* interface and on the vorticity strength. The grid spacing at the finest level was set to be $\phi/32$, where ϕ was the diameter of the bubble considered to be spherical at initial time. Five levels of refinement were used to perform the discretization of the *Eulerian* domain whose dimensions were $8\phi\times 8\phi\times Lz$, where L is the height of the domain in the z-direction, which assumes different values: $Lz = 16\phi$, $Lz = 24\phi$ and $Lz = 80\phi$.

In the first set of case studies, the ability of the method for simulating different bubble regimes was investigated while, in the second set, a series of cases in which the bubbles had the same Eotvos number (Eo) were considered to study the influence of the Morton number (M) on the Reynolds (Re) time distribution. Finally, a wobbling case study was performed based on the work of Gaudlitz & Adams (2009).

Terminal bubble shape and Reynolds number for low Reynolds flows

The ability of the current algorithm for predicting the terminal bubble shape and Reynolds number was tested against the experimental work of Bhaga & Weber (1981) for a series of low Re flows in different regimes.

A comparison with the experimental results showed that the present algorithm was able to predict the bubble shape properly. Regarding the terminal Re number, the maximum error occurred at the creeping flow regime, with a relative difference $\varepsilon = 8.62\%$. In the remaining cases, the largest errors occurred for bubbles in the skirted regime, probably due to the decrease in the bubble thickness in the skirt regions.

The influence of the Morton number on low Reynolds flows was also studied. As in the previous case, the results were checked against Bhaga & Weber (1981). The terminal bubble shape again was well predicted and the highest

relative error on the prediction of the terminal Re number occurred for the case with the lowest terminal Reynolds.

Wobbling

Two cases of wobbling bubbles were simulated in order to assess the ability of the algorithm for dealing with bubbles rising in an oscillating path. In the first case, the bubble was characterized by $Eo = 10$ and $M = 9.78 \times 10^{-8}$ and, from the Clift diagram (Clift *et al.*, 1978), $Re \approx 280$. This case was also simulated by Stene (2010), who developed a 3D algorithm based on Berger's SAMR methodology for the discretization of the *Eulerian* domain. The *Lagrangian* domain, however, followed the approach of Hua & Lou (2007), requiring two volume-recovery steps per time step.

The following physical parameters were used: $\phi = 0.0034m$, $\sigma = 0.01N/m$, $\rho_C = 1000kg/m^3$, $\mu_C = 0.0018Pa \cdot s$ and $g = 9.81m/s^2$ in the -z-direction. Density and viscosity ratios were set to 100. The *Eulerian* domain was set to $(8\phi \times 8\phi \times 80\phi)m$ and six levels of refinement were used.

According to Stene (2010), such bubble should rise following a zigzag path, which is characterized by a predominantly two-dimensional oscillating movement. Figure (1), which shows the centroid path during the simulation, shows that although the bubble follows a zigzag path at the initial stages of the flow, a transition to a spiral path takes place, and the bubble reaches the statistical steady state following this movement.

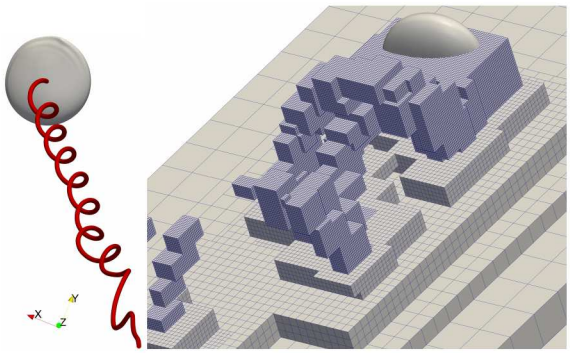

Figure 1: Left: Wobbling bubble, $Eo = 10$ and $M = 9.78 \times 10^{-8}$. Centroid path shown in 3D. The zigzag path can be seen in the beginning of the flow, and then the transition to spiral. Right: Adaptive mesh refinement based on the vorticity.

This effect is clearly seen in Fig. (2), which shows the time history of the velocity components at the bubble centroid. In the beginning of the simulation, when $t < 0.2s$, the plot clearly shows a zigzag path in the yz-plane, since the velocity magnitude is much smaller in the x-direction. However, as time evolves, this velocity component increases and, after $t = 0.4s$, x- and y- components reach a comparable magnitude. Simultaneously, the z-component of the velocity converges to an asymptotically constant value.

Figure (3) shows the Q-criterion representation of the bubble wake. An iso-surface with $Q = 5000s^{-2}$ is visualized. Hairpin unstable helicoidal eddies can be seen downstream of the bubble, as it rises in the z-direction. These eddies, which are responsible for the transition to turbulence, are similar to those found in flows over a rigid sphere.

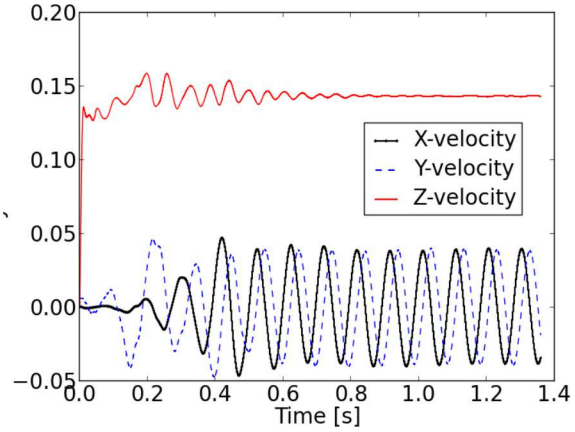

Figure 2: Wobbling bubble, $Eo = 10$ and $M = 9.78 \times 10^{-8}$. Velocity profile of the bubble centroid.

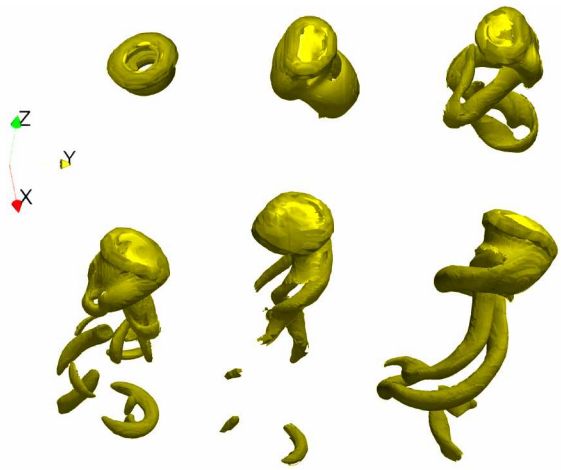

Figure 3: Wobbling bubble, $Eo = 10$ and $M = 9.78 \times 10^{-8}$. Time evolution of vortex shedding. Iso-surface shows $Q = 5000s^{-2}$.

An example of the adaptive grid can be seen in Fig. (1) on the right, depicting the three-dimensional distribution of the finest refinement level following the bubble wake.

Another unstable rising bubble was simulated based on (Gaudlitz & Adams, 2009), who studied an air bubble rising in quiescent water. The density ratio used in the reference paper was $\lambda_\rho = 774$ and the viscosity ratio employed was $\lambda_\mu = 54$. In the present work, the same viscosity ratio was used, but the density ratio was set to $\lambda_\rho = 100$. The following physical parameters were used: $\phi = 0.0034m$, $\sigma = 0.01N/m$, $\rho_C = 1000kg/m^3$, $\mu_C = 0.0018Pa \cdot s$ and $g = 9.81m/s^2$ in the -z-direction. The *Eulerian* domain was set to $(8\phi \times 8\phi \times 80\phi)m$ and six levels of refinement were used.

Figure (4) shows a temporal snapshot of the flow. An iso-surface of the Q-criterion depicts the toroidal Kelvin-Helmholtz instabilities ($Q = +5000s^{-2}$). Two iso surface of the longitudinal vorticity, $\omega_Z = \pm 50s^{-1}$, are also shown. At the lower part of the figure, the respective bubble shape at each time snapshot is shown.

The pulsating behaviour of the bubble, as illustrated in this figure, leads to the formation of Kelvin-Helmholtz instabilities in an axi-symmetric varicose mode (Lesieur, 2008). As these instabilities are relatively transported

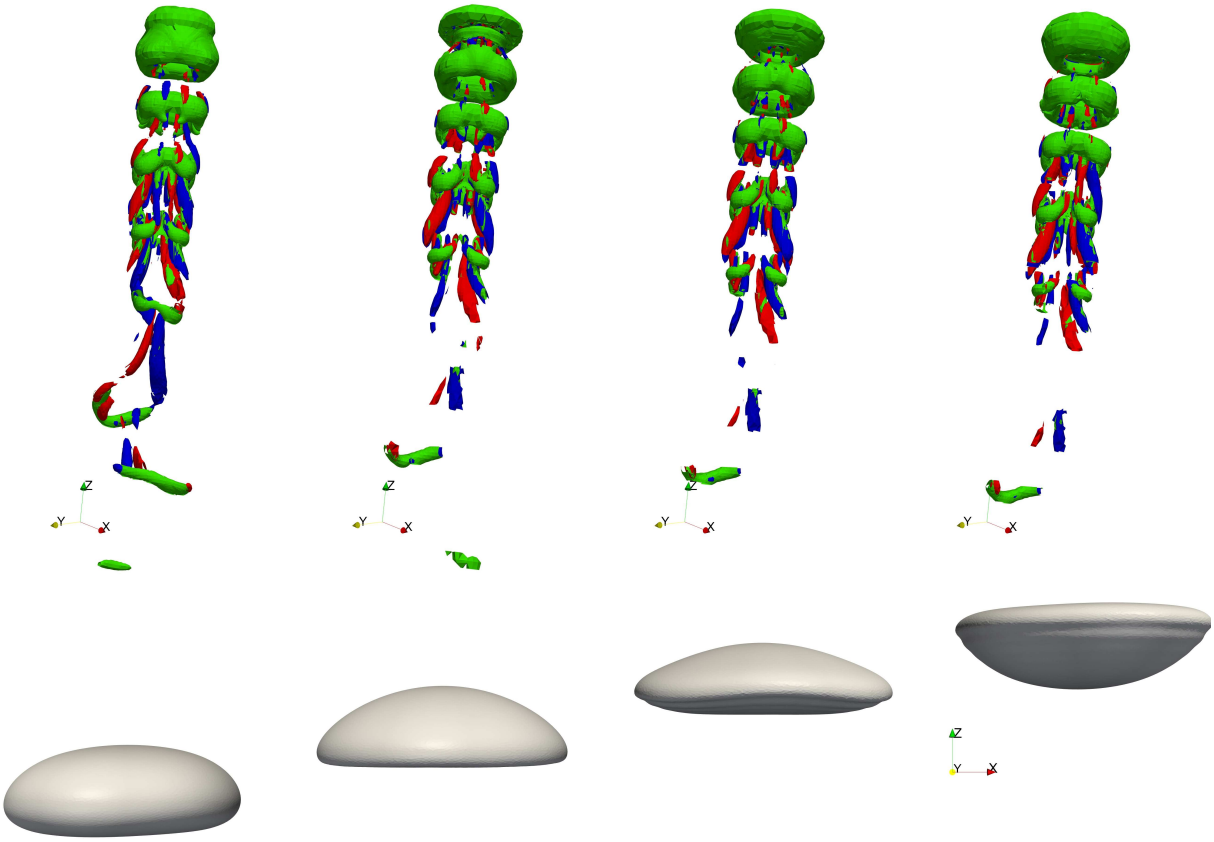

Figure 4: Pulsating wobbling. $Eo = 3.6$, $M = 2.5 \times 10^{-11}$. Top: Q-criterion $Q = 5000s^{-2}$ in green, z-vorticity in red $\omega_Z = +50s^{-1}$ and blue $\omega_Z = -50s^{-1}$. Bottom: bubble shape at the respective time instants.

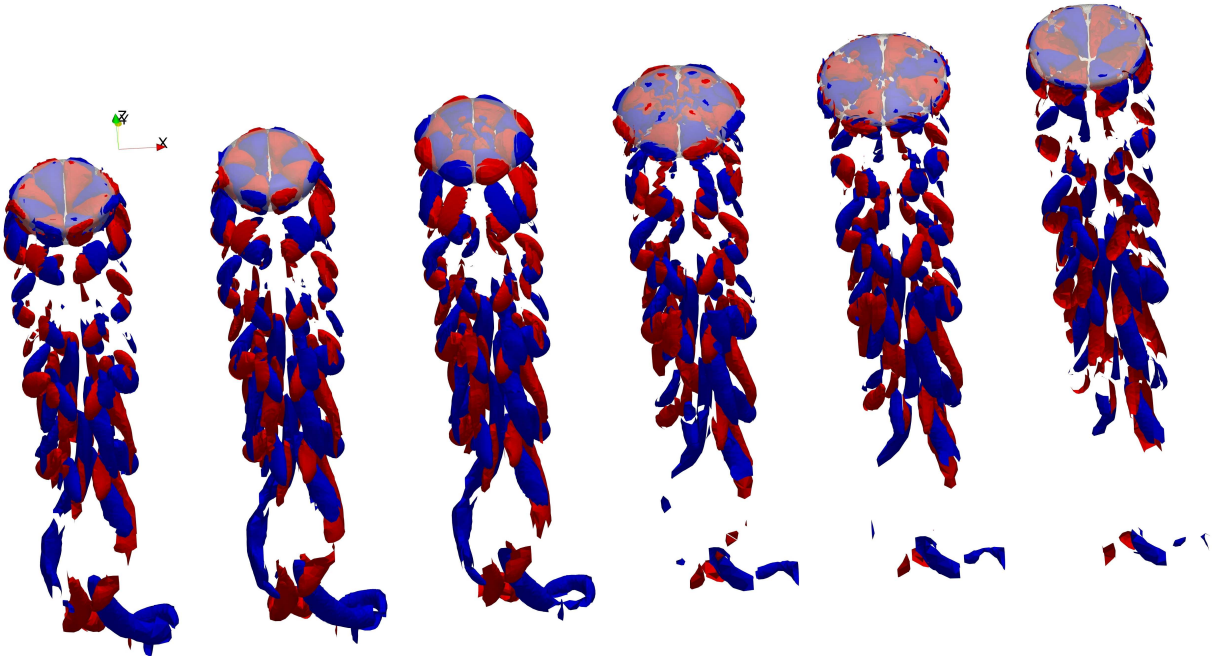

Figure 5: Pulsating wobbling. $Eo = 3.6$, $M = 2.5 \times 10^{-11}$. Iso surfaces of the z-component of the vorticity. Red=+50, blue = -50.

downstream of the bubble, another unstable mode can be identified in the azimuthal direction. These counter rotating eddies are non linearly induced by azimuthal modes of the Kelvin-Helmholtz instabilities.

Figure (5) shows unstable modes also inside the bubble, which details are shown in Fig. 6. It can be seen that these modes are in phase with the modes shown in the longitudinal, counter-rotating vortices of Fig. (4).

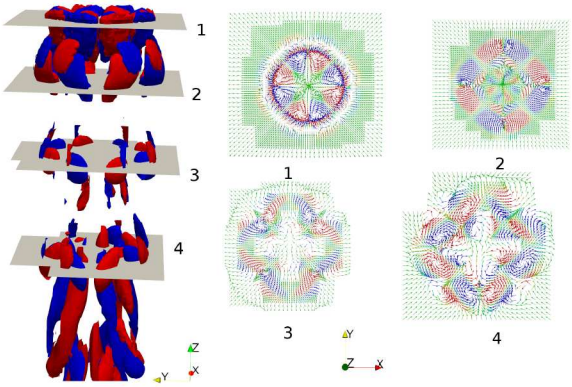

Figure 6: Pulsating wobbling. $Eo = 3.6$, $M = 2.5 \times 10^{-11}$. Left: Iso-surfaces of the z-component of the vorticity showing counter-rotating, longitudinal vortices. Right: The velocity vector field at four different planes, also shown on the left, evidencing the counter-rotating flow.

A comparative analysis between Figures (4) and (1) yields an interesting interpretation: notice that the bubble in Fig. (4) pulses, but it is not inclined with relation to the z-direction. The bubble in Fig. (1), on the other hand, rotates around the z-axis. As a result, the vortex shedding by the bubble in Fig. (4) occurs in the varicose mode, which remains stable while the bubble path remains rectilinear. Fig. (1), on the other hand, depicts a vortex shedding in a sinuous mode, as can be seen in Fig. (3), owing to the oscillating bubble path. This kind of result is delivered by what is currently called numerical, or virtual, experimentation. Allied to the material experimentation, this methodology gradually leads to a better understanding of nature and, as a consequence, to control and reproduce natural phenomena.

The varicose instabilities highlighted in the present work are attributed to these pulsations, since they are extremely difficult to sustain in material experiments as well in virtual, or computational, experiments. The high level of physical details captured by the present simulations enhances the potential of the AMR methodology implemented in the computational code of the present work. This kind of result has a high scientific value for explaining and understanding the process of transition to turbulence in the wakes generated by bubbles in two phase flows.

CONCLUDING REMARKS

A fully adaptive Front-Tracking Method was presented in the present work, aiming at the simulation of three-dimensional bubbly flows. The use of an adaptive mesh refinement strategy for the solution of the Navier-Stokes equations enabled local detailing of the flow.

The remeshing algorithm applied to the *Lagrangian* mesh yielded good results, since it intrinsically preserves the geometry shape and dimensions, therefore preserving the volume. However, the non-conservative interpolation of the velocity field required an additional volume recovery algorithm. Also, cases simulated during the sensitivity analysis showed the presence of non-physical undulations, a phenomena also reported by other authors. In this sense, the TSUR-3D algorithm (Sousa *et al.*, 2004) succeeded on preventing such phenomena while still preserving the bubble shape.

The density ratio has shown little influence on the rise of bubbles at low Reynolds numbers. As the Reynolds number increases, its influence grows and interferes on the bubble path, even preventing the transition to an oscillating path in the case of wobbling bubbles.

Regarding the low Reynolds simulations, the terminal bubble shape and Reynolds number were in good agreement when compared to the experimental references. The errors shown in cases simulating skirted bubbles can be attributed to the skirt width at the terminal regime.

The initial bubble shape led to two different behaviours in low and high Re flows. While in the first case all bubbles converged to the same terminal shape and Re number, flows at moderate Re have shown to be very sensitive to the initial bubble shape, leading to toroidal bubbles as the initial aspect ratio increased.

Finally, two cases were simulated for bubbles in the wobbling regime. In the first case, the bubble initially described a zigzag path. As time evolved, the bubble path changed from zigzag to spiral and then achieved a steady state under this trajectory. In the second case, the bubble ascended describing an almost linear path. The bubble shape oscillated following a pulsation pattern, and the vortex shedding followed a varicose mode. The instabilities inside the bubble interact non-linearly with the external Kelvin-Helmholtz instabilities, creating the longitudinal counter rotating filaments.

ACKNOWLEDGEMENT

This work was sponsored by PETROBRAS (Cooperation Agreements n. 0050.0022712.06.5 / 4600277717 and n. 0050.0022712.06.4/4600278528), FAPEMIG (process n. APQ-259710) and CNPq (processes nn. 471929/2010-7 and 309433/2011-8). Also, the authors are in debt with Prof. Antonio Castelo Filho, from the University of São Paulo at São Carlos, for the fruitful discussions about local surface smoothing algorithms.

REFERENCES

Bhaga, D. & Weber, M. E. 1981 Bubbles in viscous liquids: shapes, wakes and velocities. *Journal of Fluid Mechanics* **105**, 61–85.

Brennen, Christopher Earls 2005 *Fundamentals of Multiphase Flow*. California: Cambridge University Press.

Ceniceros, H.D. & Roma, A.M. 2005 A multi-phase flow method with a fast, geometry-based fluid indicator. *Journal of Computational Physics* **205** (2), 391 – 400.

Clift, R., Grace, J. R. & Weber, M. E. 1978 *Bubbles, Drops and Particles*. New York: Academic Press.

Gaudlitz, Daniel & Adams, Nikolaus A. 2009 Numerical investigation of rising bubble wake and shape variations. *Physics of Fluids* **21** (12), 122102.

Hua, Jinsong & Lou, Jing 2007 Numerical simulation of bubble rising in viscous liquid. *Journal of Computational Physics* **222**, 769–795.

Lesieur, M. 2008 *Turbulence in Fluids*. Springer.

Mauch, S. 2003 Efficient algorithms for solving static hamilton-jacobi equations. PhD thesis, Caltech, Pasadena CA.

Peskin, C. S. 1977 Numerical analysis of blood flow in the heart. *Journal of Computational Physics* **25** (1), 220–252.

Peskin, C. S. 2002 The immersed boundary method. *Acta Numerica* **11**, 479–517.

Roache, P. J. 1998 *Verification and Validation in Computational Science and Engineering*. Hermosa Publishers.

Shin, S. & Juric, D. 2002 Modeling Three-Dimensional multiphase flow using a level contour reconstruction method for Front Tracking without connectivity. *Journal of Computational Physics* **180**, 427–470.

Sousa, F.S., Mangiavacchi, N., Nonato, L.G., Castelo, A., Tomé, M.F., Ferreira, V.G., Cuminato, J.A. & McKee, S. 2004 A front-tracking/front-capturing method for the simulation of 3d multi-fluid flows with free surfaces. *Journal of Computational Physics* **198** (2), 469–499.

Stene, J. F. 2010 Numerical simulation of interfacial and multiphase flows using the front tracking method. PhD thesis, National University of Singapore.

Tryggvason, G., Bunner, B., Esmaeeli, A., Juric, D., Al-Rawahi, N., Tauber, W., Han, J., Nas, S. & Jan, Y. J. 2001 A front-tracking method for the computations of multiphase flow. *Journal of Computational Physics* **169**, 708–759.

Tryggvason, G., Scardovelli, R. & Zaleski, S. 2011 *Direct Numerical Simulations of Gas-Liquid Multiphase Flows*. Cambridge, UK: Cambridge University Press.

Unverdi, S. A. & Tryggvason, G. 1992 A front-tracking method for viscous, incompressible, multi-fluid flows. *Journal of Computational Physics* **100**, 25–37.

de Vries, A. W. G. 2001 Path and wake of a rising bubble. PhD thesis, University of Twente, Enschede.